

UGC 3995: A CLOSE PAIR OF SPIRAL GALAXIES¹

P. Marziani

Osservatorio Astronomico di Padova, Padova, Italia

e-mail: marziani@pd.astro.it

M. D' Onofrio

Dipartimento di Astronomia, Università di Padova, Padova, Italia

e-mail: donofrio@pd.astro.it

D. Dultzin-Hacyan

Instituto de Astronomía, UNAM, Apto. Postal 70-264, México, D. F. 04510, México

e-mail:deborah@astroscu.unam.mx

J. W. Sulentic

Department of Physics & Astronomy, University of Alabama, Tuscaloosa, USA

e-mail:giacomo@merlot.astr.ua.edu

ABSTRACT

UGC 3995 is a close pair of spiral galaxies whose eastern component hosts a Seyfert 2 nucleus. The object was selected because a bright filamentary structure that apparently connects the nuclei of the two galaxies made it a good candidate to investigate a possible interaction–AGN connection. We present a detailed analysis of this system using long slit spectroscopy and narrow ($H\alpha + [NII]\lambda\lambda 6548, 6583$) as well as broad band (B, R) imaging and an archive WFPC2 image. The component galaxies reveal surprisingly small signs of interaction considering their spatial proximity and almost identical recession velocities, as the bright filament is probably an optical illusion due to the superposition of the bar of the Seyfert galaxy and of the spiral arms of the companion.

The broad band morphology, a B–R color map, and a continuum-subtracted $H\alpha + [NII]\lambda\lambda 6548, 6583$ image demonstrate that the western component UGC 3995B is in front of the Seyfert-hosting component UGC3995A, partly obscuring its western side. The small radial velocity difference leaves the relative motion of the two galaxies largely unconstrained. The observed lack of major tidal deformations, along with some morphological peculiarities, suggests that the

¹Based on Observations collected at San Pedro Martir, Baja California, México.

galaxies are proximate in space but may have recently approached each other on the plane of the sky. The geometry of the system and the radial velocity curve at P. A. $\approx 106^\circ$ suggest that the encounter may be retrograde or, alternatively, prograde before perigalacticon.

The partial overlap of the two galaxies allows us to estimate the optical thickness of the disk of component B. We derive an extinction ≈ 0.18 visual magnitudes in the intra-arms parts of the foreground galaxy disk, and $\gtrsim 1 - 1.5$ visual magnitudes in correspondence of the spiral arms.

Subject headings: galaxies: active — galaxies: individual (UGC 3995) — galaxies: interactions — galaxies: kinematics and dynamics — galaxies: photometry — galaxies: Seyfert — galaxies: structure

1. Introduction

Gravitational interactions have been proposed as a triggering mechanism for Seyfert-type activity since the early 70's. The interaction-AGN connection is now part of the standard paradigm of active galactic nuclei (AGN; see Dultzin-Hacyan et al. 1999a, Stockton 1999, Osterbrock 1993, De Robertis, Yee & Hayhoe 1998, Blandford 1990, for recent discussions emerging from different perspectives). Gravitational disturbances are expected to be effective in transferring angular momentum on scales of hundreds of parsecs (e. g. Begelman 1994, and references therein), even though observational tests have produced somewhat sparse or mixed results. The AGN-interaction connection has been investigated following two main observational approaches: *statistical*: counts of the number of galaxies near to galaxies hosting Seyfert nuclei and *specific*: studies of the kinematics and dynamics of ionized gas in spiral disks and circumnuclear regions of individual Seyferts. Both methods have drawbacks: present-day observational techniques are not ideal for large scale studies that are needed for a proper survey of companions within ~ 1 Mpc, and we are unable to resolve structure within which nuclear activity seems to be confined ($\lesssim 1$ pc). Several statistical papers based on sky surveys have added important insight, even if some of them obtained contradictory results (Laurikainen & Salo 1995; Dultzin-Hacyan et al. 1999a analyze the origins of such disagreement). The most firm result is probably a significant excess of bright companions in the vicinity of Seyfert 2 galaxies (Dultzin-Hacyan et al. 1999b, Dultzin-Hacyan et al. 1999a, Laurikainen & Salo 1995). Restricting the attention to dynamical studies of disk gas, direct observational evidence in favor of interaction-driven neutral, molecular or ionized gas infall toward the nucleus on scale of several hundreds of

parsecs remains scant. Successful observations require a special time in the evolution of an interacting system, and detailed observations of gas morphology and kinematics. Perhaps only in the triple system NGC 7592 spectroscopic evidence of ionized gas infalling toward the Seyfert nucleus has been convincingly found (Rafanelli & Marziani 1992).

UGC 3995 was selected as part of a larger investigation on the effects of interaction on the gaseous component in a small set of galaxies where activity might have been induced by mass-transfer of tidally stripped gas from a companion. UGC 3995 is a bright pair of spiral galaxies with partially overlapping disks and negligible redshift difference that, at first glance, offers the possibility of direct evidence in favor of tidal stripping and/or more quiescent cross fueling into an active nucleus: a bright filament appears to connect the Seyfert 2 nucleus of UGC 3995A with the nucleus of UGC 3995B over ≈ 29.2 arcsec of angular distance, which corresponds to ≈ 9 kpc of projected linear distance (see Fig. 1; from the heliocentric radial velocity of UGC 3995A, $v_r \approx 4746$ km s $^{-1}$, we compute a distance ≈ 63.3 Mpc; $H_0 = 75$ km s $^{-1}$ Mpc $^{-1}$ is assumed thorough the paper). The earliest investigations pointed out the peculiar nature of UGC 3995. UGC 3995 has been included in the catalog of isolated pairs of galaxies (CPG 140, Karachentseva 1973) where it is assigned the strongest interaction class LIN(br+ta) intended to indicate the presence of tidal tails and bridges. The “bridge” is the bright filament seen in Fig. 1. UGC 3995 was also listed as part of an isolated triplet, because a third galaxy (MCG +05–19–003) of comparable brightness is located ≈ 4 arcmin NW (Karachentseva et al. 1988). Keel 1985 first identified the nucleus of UGC 3995A as having Seyfert 2 properties; he suggested that the UGC 3995 system was “a close pair of spirals one of which has a type 2 Seyfert nucleus and apparent knotty jet”. More recently, a report based on integral field spectroscopy, and high spatial resolution (Chatzichristou, Vanderriest & Lehnert 1998) suggested that gas may be infalling toward the active nucleus in the central regions of the UGC 3995 system.

From our data, unambiguous evidence for interaction and gas transfer is difficult to find in the UGC3995 pair. UGC 3995, in fact, illustrates many of the difficulties of unambiguously proving interaction even for a very close pair of spirals with almost identical redshift. § 2 summarizes our data and the reduction procedures employed. § 3 presents the main observational results of this investigation. § 4 considers UGC 3995 in the light of generally accepted morphological, spectroscopic and photometric indicators of interaction. Preliminary results of this investigations were presented in Dultzin-Hacyan, Marziani & D’Onofrio 1998.

2. Observations and Data Reduction

Narrow (redshifted $H\alpha + [NII]\lambda\lambda 6548,6583$ (filter width $\approx 70 \text{ \AA}$) and broad-band (R, B) images of UGC 3995 were obtained on January 30, 1995 at the Cassegrain focus of the 2.1 m telescope of the Observatorio Astronomico Nacional at San Pedro Martir (SPM), B. C., México. A Tektronix CCD ($24 \mu\text{m}$ square pixel size, 1024×1024 format) employed as a detector yielded a scale of $0.315 \text{ arcsecs/pixel}$ and a field of view of $\approx 5.4 \text{ arcmin}$. Long slit spectra were collected with the 2.1 m SPM telescope on Dec. 9, 1994 ($H\beta$ spectral region) and on February 2–4, 1995 ($H\alpha$ region) using a B&Ch spectrograph, with the same Tektronix detector. The December 1994 observations were obtained with a 400 lines/mm grating and covered the usable range from $3900\text{--}6720 \text{ \AA}$, with a resolution $\approx 7 \text{ \AA FWHM}$. A 1200 lines/mm grating was employed in January and February 1995 for observations of the $H\alpha$ region. The slit width was $200 \mu\text{m}$ at the focal plane of the telescope (2.6 arcsecs). This setup resulted in a resolution of $\approx 2 - 2.2 \text{ \AA FWHM}$. Table 1 provides a log of observations, reporting the date and universal time for each exposure, the exposure time, the filter or the spectral range in case of spectra, and, for spectra, the position angle of the slit. A 500-s image obtained with the HST WFPC2 through the “wide visual” F606W filter on May 17, 1994 was also retrieved from the HST data archive (dataset U2E65T01T see Malkan, Gorjian, & Tam 1998 for a full presentation of that data). Part of the mosaiced image is shown in Fig. 2.

2.1. Data Calibration

Broad Band Images Images obtained with the same filter were registered and co-averaged to improve S/N and to remove cosmic rays. Transformation from the instrumental to the Johnson photometric system was achieved using a set of CCD standard stars in the globular cluster NGC 4147 (Odewahn et al. 1992). To compute the total luminosity of the galaxy, we constructed growth curves by integrating the flux through circular apertures, adopting the zero point and color terms derived from the standard stars.

Narrow Band Images Flux calibration of narrow band images was obtained by observing a spectrophotometric standard star through the narrow band filter. After bias subtraction and flat field correction, the average R band-image was scaled and subtracted to the average narrow band image to eliminate the continuum underlying the $H\alpha + [NII]\lambda\lambda 6548,6583$ blend. The resulting “pure” $H\alpha + [NII]\lambda\lambda 6548,6583$ image is shown in Fig. 3. Uncertainties associated with the photometric calibration and underlying continuum subtractions are estimated to be within $\pm 20 \%$.

Spectra Wavelength calibration of science spectra was obtained from HeAr comparison spectra, taken between or after pairs of 30 minute exposures with the same settings. The final wavelength zero point was checked against the wavelength of strong sky lines (Marziani 1995). An average shift of about $\Delta v_r \approx 10 \text{ km s}^{-1}$ was taken into account. Flux calibration was obtained by the observation of tertiary standard stars, with two sequence of exposures taken at widely different times during each night of the December and January observing runs. Standard stars were observed with the slit opened to $\approx 500 \mu\text{m}$ in order to minimize light losses.

3. Results

3.1. Broad Band Morphology

Our R-band image (Fig. 1) suggests that the distorted appearance of the bright filament joining UGC 3995A and UGC 3995B is almost entirely due to the foreground spiral arms of UGC 3995B (and to dust lanes associated with them), which cross the hammer-shaped bar like sickle blades. The eastern spiral arm of UGC 3995A obscures the bar of UGC3995A at its NW end, creating the illusion of a filamentary region (the highest surface brightness part of the bridge, which appear “semi-detached” from the inner part of the UGC 3995A bar) in between the nuclei of UGC 3995A and B (clearly visible in both Fig. 1 and 2). The bar looks rather symmetric, but some intrinsic asymmetry is associated with that “semi-detached” region, which appears to extend the NW end of the UGC 3995A bar more than expected if the bar ends are symmetric with respect to the nucleus. The overall scenario is validated, with a much greater extent of spatial details (including several arm branches not visible in the ground based observations), by the WFPC2 image (Fig. 2). In addition to the eastern arm of UGC 3995A, the western arm of UGC 3995B can be followed as it winds around the galaxy and also crosses UGC 3995A not far from the nucleus, where a prominent dust lane appears to cut across the circumnuclear regions.

3.2. Broad Band Photometry

The first rows of Table 2 report the integrated B, and R magnitudes computed using the growth curve method, with an expected uncertainty of $\approx 0.1 \text{ mag}$. Following de Vaucouleurs et al. 1991, if we apply a galactic extinction toward UGC 3995 of 0.09 magnitudes, at the adopted distance of 63.3 Mpc the absolute magnitude of the whole system is $M_B \approx -21.6 \text{ mag}$.

Models of the Two Dimensional Surface Brightness Distribution In order to recover the individual photometric properties of the two galaxies, we constructed a set of two dimensional models of their light distribution. This was achieved by fitting only the regions of the frame dominated by each galaxy separately. Regions including foreground stars and substructures such as the bar, the knotted spiral arms, the Seyfert nucleus and the nucleus of UGC 3995B (nuclear regions are dominated by seeing) were excluded from the fit by masking frames. We modeled the 2D surface brightness distribution of the galaxies with bulge and disk components represented by concentric ellipses whose apparent flattening is due to the inclination with respect to the line of sight (see Byun 1995, D’Onofrio et al. 1999 for references). The bulge and the disk light distribution are given respectively by:

$$\mu_b = \mu_e + k \times [(R_b/r_e)^{1/n} - 1] \quad (\text{bulge}) \quad (1)$$

$$\mu_d = \mu_0 + 1.086 \times (R_d/r_h) \quad (\text{disk}) \quad (2)$$

where $R_b = \{[(x_i)]^2 + [y_i/(b/a)_b]^2\}^{(1/2)}$ and $R_d = \{[(x_i)]^2 + [y_i/(b/a)_d]^2\}^{(1/2)}$ are the distances of the pixel (i, j) from the galaxy center. The light profile of the bulge follows a $r^{1/n}$ law (Caon, Capaccioli & D’Onofrio 1993), while the disk has an exponential distribution. The bar of UGC 3995A and the spiral arms have not been modeled.

Table 2 provides the results obtained for two “best fitting” models (yielding minimum χ^2). Since the solution is not unique but depends on the choice of the masking frame, our ‘fiducial solutions’ are two models that give the best residuals, a good behaviour of the global growth-curve for two extreme, but equally reasonable choices of the masking frames. Other choices of the masking frames are expected to give results intermediate between model I and II. Finally, from the overall appearance and the bulge/disk decomposition performed, we suggest a morphological type SBbc (or SB(r)bc) for UGC 3995A and Sc (or Sd) for UGC 3995B.

B–R Color Map The B – R color map (Fig. 5) allows us to trace the northern and southern spiral arms of UGC 3995A as elongated blue features ($B - R \approx 0.5 - 0.6$). The bar appears redder than the bulge (average B–R, including the nuclear region, is 1.28 ± 0.05). UGC 3995B appears of rather bluer color index ($B - R \approx 0.7$), which suggests the absence of appreciable obscuration. The area in between the nuclei is confused by the superposition of the NW end of the bar in UGC 3995A with the eastern arm of B. A comparison between the R and B–R images (and the HST image) confirms that the spiral arms of UGC 3995B are obscuring the western side of the UGC 3995A bar. The extension of the western spiral

arm of UGC 3995B is most likely responsible for the reddish region that is elongated perpendicular to the bar.

3.3. Emission Line Morphology & Photometry

The broad band morphology can be easily compared to the morphology of the ionized gas, which results from the $H\alpha + [NII]\lambda\lambda 6548,6583$ map shown in Fig. 3. The prominent bulge and the bar of UGC 3995A almost completely disappears in the narrow band image, where most emission can be ascribed to (i) the galactic nuclei, (ii) knots associated to the spiral arms of either galaxies, (iii) weak $H\alpha$ diffuse emission. The absence of strong unresolved, diffuse $H\alpha$ emission is confirmed by our long slit spectra at P.A. = 45° , and 125° : $H\alpha$ emission on the eastern side of UGC 3995A is, for example, detected only in correspondence of spiral arms or knots. Table 3 lists region label, position with respect to UGC 3995A, and fluxes. Fig. 4 identifies each emitting region with a number in rough order of decreasing right ascension. Diffuse emission is weak but not negligible, since emission that cannot be ascribed to discrete sources listed in Tab. 3 appear to contribute to $\lesssim 1/2$ of the total $H\alpha + [NII]\lambda\lambda 6548,6583$ emission. The diffuse emission is subject to an uncertainty which is estimated to be $\lesssim 50\%$, larger than that of the flux of discrete sources ($\approx 20\%$).

The knots on the eastern spiral arm of UGC 3995B, and several knots of the northern arm of UGC 3995A create the appearance of a ring, which is an optical illusion due to a chance peculiar orientation of the two spiral arms. It is important to note, in this respect, that the knot at the center of this pseudo-ring (labeled 13) is not the nucleus of UGC 3995B, which is knot 15, located at the center of symmetry of the spiral arms of UGC 3995B. This is seen clearly comparing Fig. 3 and Fig. 1, which have the same scale. The knot 13 at the center of the pseudo-ring cannot be attributed to any of the spiral patterns of the two galaxies. This region is located at the end of the high surface brightness extension of the UGC 3995A bar NW tip. The main features emerging from the previous analysis are sketched in Fig. 6.

3.4. Nuclear Spectroscopy

UGC 3995A The nucleus of component A shows a type 2 Seyfert spectrum (Keel 1985). Fig. 7 shows the flux calibrated nuclear spectrum (in the rest frame of the galaxy, not corrected for galactic extinction) from 3800 to 7200 Å. Measurement of the lines

in the UGC 3995A are reported in Table 4. The radial velocity, measured from $H\alpha$, $[\text{NII}]\lambda\lambda 6548,6583$, $[\text{SII}]\lambda\lambda 6716,6730$, and $H\beta$ and $[\text{OIII}]\lambda 4959,5007$ lines in all our best spectra is $v_{r,\text{hel}} = 4746 \pm 18 \text{ km s}^{-1}$, where the uncertainty is at 2σ confidence level. This determination agrees with the value $v_{r,\text{hel}} \approx 4747 \text{ km s}^{-1}$ obtained from the HI 21-cm profile (Sulentic & Arp 1983; see Fig. 9). The spectral energy distribution shown in Fig. 7 suggests an overall spectral type of G2 ($\text{EW}(H\beta)$ in absorption $\approx 1.59 \text{ \AA}$, summed over $\approx 7''$).

UGC 3995B In Table 4 only the fluxes for $H\alpha$, $[\text{NII}]\lambda 6583$, and $[\text{SII}]\lambda\lambda 6716,6730$ are reported. A spectrum at P.A. = 103° kindly provided us by W. C. Keel shows $[\text{OIII}]\lambda 5007/H\beta \approx 0.20 \pm 0.05$ confirming that the spectrum is of a low-ionization nuclear HII region. The radial velocity of the single, middle peak in the 21 cm HI profile ascribed to UGC 3995B (see next paragraph, §3.5) is $v_{r,\text{hel}} \approx 4748 \text{ km s}^{-1}$. The spectra obtained at P.A. = 106° yield a radial velocity $v_{r,\text{hel}} \approx 4766 \pm 16 \text{ km s}^{-1}$, exceeding by 27 km s^{-1} that of UGC 3995A (the excess is much larger than the internal consistency errors of our spectra), in fair agreement with the HI determination.

3.5. Spectroscopy of Extended Emitting Regions

Four co-averaged 30 min. exposures yielded the long slit extended $H\alpha + [\text{NII}]\lambda\lambda 6548,6583$ spectrum shown in Fig. 8. On the western side of UGC 3995A (upper part of Fig. 8) the strongest emission is due to gas in the disk of UGC 3995B. Emission from UGC 3995A is very weak, because of obscuration by the foreground disk of UGC 3995B. Only the $H\alpha$ knot on the higher velocity side (region 13) and the very faint and extended $[\text{NII}]\lambda 6583$ emission can be associated to UGC 3995A. This interpretation is made more obvious by the radial velocity curve at P. A. $\approx 106^\circ$ (left panel of Fig. 9), obtained from measurements on the spectrum shown in Fig. 8. The nearly flat radial velocity curve to the West is due to the brighter $H\alpha$ and $[\text{NII}]\lambda\lambda 6548,6583$ emission in Fig. 8, and is consistent with a galaxy observed nearly face-on, as it is the case of UGC 3995B. The inclination of UGC 3995B can be estimated from the slope of the radial velocity curve. Assuming an average slope for Sc galaxies of $37 \text{ km s}^{-1} \text{ kpc}^{-1}$ in the inner part of the rotation curve (Rubin et al. 1980), we obtain $i(\text{UGC 3995B}) = 8^\circ \pm 2^\circ$. The high velocity part of the radial velocity curve is due to the western side of the UGC 3995A disk which is heavily obscured. Consistently, its radial velocity is close to that of the high velocity horn in the HI 21 cm line profile (right panel of Fig. 9, from Sulentic & Arp 1983).

It is noteworthy that for UGC 3995B we observe both $H\alpha$ and $[\text{NII}]\lambda\lambda 6548,6583$, with the first stronger, as expected from normal disk HII regions (the HII nature of the UGC

3995B knots across the slit at P. A. =106° is confirmed by a spectrum provided us by W. C. Keel, which shows $[\text{OIII}]\lambda 5007/\text{H}\beta \lesssim 0.5$ for the extended emission). On the contrary, for UGC 3995A we observe (save in region 13) $[\text{NII}]\lambda 6583$ but no $\text{H}\alpha$, which most likely falls below 3σ the noise level. This implies that the ratio $[\text{NII}]\lambda 6583/\text{H}\alpha$ is $\gg 1$, possibly $\gtrsim 2.5$. Appreciable $[\text{NII}]\lambda 6583$ emission without $\text{H}\alpha$ is observed on the eastern side of UGC 3995A as well, up to ≈ 10 arcsec from the nucleus (see Fig. 8). A possible cause may be related to an ionization cone (Chatzichristou, Vanderriest & Lehnert 1998). It is unlikely that extended $[\text{NII}]\lambda 6583$ emission is due exclusively to under/over subtraction of sky continuum/lines or other instrumental effects, especially on the western side of UGC 3995B. There is also some evidence for an $[\text{NII}]\lambda 6583$ emitting filament on the western side of UGC3995A (barely visible in Fig. 8) within 10 arcsecs from the nucleus. This emission appears to join the high velocity end of UGC3995A nuclear emission with the $[\text{NII}]\lambda 6583$ emission associated with UGC 3995B (it gives rises to the “curl” at the eastern end of the UGC 3995B radial velocity curve, Fig. 9). The weakness of the high velocity $[\text{NII}]\lambda 6583$ extended emission makes it desirable that confirmatory data be obtained.

3.6. The Optical Thickness of UGC 3995B

The UGC 3995 system is one of the rare cases in which one galaxy appears in foreground of another, without any gross morphological disturbance. The optical thickness of galaxy disks has been a hot topic in recent years (Valentijn 1990, White & Keel 1992, James & Puxley 1993, Domingue, Keel & White 1998), since recent results suggest significant optical depth, at variance with early studies (Holmberg 1958, de Vaucouleurs 1959). White & Keel 1992 have argued that the optical thickness is highly variable across a spiral disk and our images (especially WFPC2) of UGC 3995 support this view. The problem cannot be extreme, as the northern spiral arm of UGC 3995A can be traced in the region behind UGC 3995B. An estimate of the absorption $\langle A_V \rangle$ of the Sc galaxy UGC 3995B can be obtained directly from the broad band WFPC2 image. If the UGC 3995A bar is roughly symmetric across the nucleus and unperturbed (which seems to be the case save at its NW end), then the galaxy surface brightness measured along the bar axis should be the same in both directions. We subtracted a model of component B to the WFPC2 image; we then extracted the photometric profile *along the bar* across the Seyfert nucleus. The photometric profile on the obscured side was then divided by the folded photometric profile of the unobscured side. The results is shown in Fig. 10. Absorption in the inter-arm region between the extension of the western arm and the eastern arm is fairly constant (UGC3995A appears to be dimmed as if seen through a screen of absorbing matter), the median $\langle A_V \rangle$ being ≈ 0.18 , with intrinsic scatter ± 0.09 mag (2σ), in good agreement with

the values found for other spirals (Domingue, Keel & White 1998). A_V is much higher in correspondence of the spiral arms: 0.9 mag. and 1.4 mag for the western extension and for the eastern arm respectively (at ≈ 1 arcsec and 5 arcsec in Fig. 10). Absorption is quite patchy in both the interarm region and in the spiral arms. In correspondence of the darkest patches on the dust lanes, A_V is estimated to be in the range 2–4 magnitudes.

We considered also two approaches based on our spectra at P.A.=106°: (a) we assume that the integrated [NII] λ 6583 intensity is intrinsically the same on the eastern (unobscured) and western (obscured) side of UGC 3995A; we obtain $I([\text{NII}]\lambda 6583)_{\text{East}}/I([\text{NII}]\lambda 6583)_{\text{West}} \approx 0.37$, which corresponds to $A_V \approx 1.33$; (b) if we do the same assumption for the H α integrated emission we obtain $I(\text{H}\alpha)_{\text{East}}/I(\text{H}\alpha)_{\text{West}} \approx 0.31$, thus A_V results ≈ 1.59 . The average of these values is $\langle A_V \rangle \approx 1.46$, in good agreement with estimates for other spirals from the Balmer decrement (James & Puxley 1993), and in agreement with our estimate for the spiral arms. Due to the patchiness of absorption, and to selection effects which favor the brightest HII regions, the value obtained from the spectra should be considered as an upper limit. Additional caution is warranted by the possible variation of ionization conditions across the disk of UGC 3995A (§3.5).

4. Discussion

4.1. Absence of Strong Tidal Effects

There is little evidence in the broad-band ground-based or HST images for features that can be unambiguously assigned to the effects of a strong tidal field. No evidence of *connections* is seen in the narrow band image (Fig. 3). Taking into account the confusion due to overlap of the two galaxies, the spiral arms of UGC 3995B appear nearly symmetric with respect to the nucleus and with no evident sign of perturbation.

The HI velocity profile is remarkably regular, if compared to several interacting galaxies also studied by Sulentic & Arp 1983. A reasonably straightforward deconvolution of that profile is possible because UGC 3995A and B show considerably different inclinations to the line of sight (Fig. 9). Component A shows a “double-horn” profile characteristic of a fairly massive inclined spiral galaxy. A third horn is detected near the center of the broad ($\Delta v_r = 476 \text{ km s}^{-1}$) double horn that is most simply ascribed to the single-peaked emission from the near face on component B. The sides of the broader profile are quite steep and characteristic of an undisturbed HI disk in a spiral galaxy. Sulentic & Arp 1983 present a qualitative classification of HI profiles in terms of evidence for gravitational disturbance. In that scheme UGC3995 is normal except for the presence of the third peak. If the HI disk is

sensitive to dynamical perturbations from near neighbors, interaction has not yet produced any appreciable disturbance of the HI profile. Simulations show that disk HI gas is the most component most sensitive to tidal forces (e. g. Combes 1997, and references therein).

The total line luminosity for the UGC 3995 system measured from the continuum subtracted narrow band image (Fig. 3) is $L(\text{H}\alpha + [\text{NII}]\lambda\lambda 6548, 6583) = 2.8 \times 10^{41}$ ergs s^{-1} . If we subtract the contribution from the Seyfert nucleus, and assume a ratio $[\text{NII}]\lambda\lambda 6548, 6583/\text{H}\alpha \approx 0.5$, $L(\text{H}\alpha) = 1.5 \times 10^{41}$ ergs s^{-1} . This corresponds to a total star formation rate SFR between $0.1 - 100 M_{\odot} \approx 1 M_{\odot}\text{yr}^{-1}$ which is far below the SFR of classical starburst galaxies. The luminosity of the brightest emitting regions in both galaxies are not extraordinary for late-type spirals (e. g., Kennicutt, Edgar, & Hodge 1989). The $\text{H}\beta$ absorption EW value is also consistent with the absence of a young stellar population (Bressan et al. 1996).

4.2. Evidence of Weak Tidal Disturbances

The components of UGC3995 are proximate on the sky and in redshift but our images fail to confirm any obvious *strong* tidal feature, as well as enhanced star formation. We do find several second-order features that suggests that the two galaxies are not double simply because of a chance superposition (as in the case of NGC 3314; Schweizer & Thonnard 1985 where two galaxies of different redshift appear overlapping, or of a widely separated pair at roughly the same distance from the Galaxy), but that they are actually proximate in space and physically interacting: (1) emission knots in the spiral arm of UGC 3995B on the side towards A are much brighter than those on the opposite side; (2) emission knot 13 (see Fig. 3); (3) the appearance of the northern spiral arm of UGC 3995A; (4) the “semi-detached” region at the NW end of the UGC3995A bar; (5) a possible extension and distortion of the western spiral arm of UGC3995B, which is appreciable especially in the HST image (Fig. 2).

Point (1) is the strongest evidence in favor of appreciable tidal effects. $\text{H}\alpha$ images are somewhat sparse in the literature, and most intensity information is lost in print, so that a systematic and accurate comparison between UGC 3995 and other systems is not possible. Inspection of published $\text{H}\alpha$ images (for examples those by Hodge 1975a; Hodge 1975b; Hodge & Kennicutt 1983, Ryder & Dopita 1993) suggest that the distribution of HII regions in isolated late-type spirals are usually rather symmetric. Contrarily bright arc-like features are found in several interacting objects (e.g. UGC 4081, Chatzichristou, Vanderriest & Lehnert 1998; NGC 7469, Marquez & Moles 1994, Pronik & Metik 1990), although not always on the side towards a companion. Surveys of the distribution of HII regions

confirm that bridges and arcs of prominent $H\alpha$ emission are more frequent in peculiar and interacting galaxies. The $H\alpha$ asymmetry in the arms of UGC 3995B is *very strong* and similar to the kind seen in the cited interacting systems. The $H\alpha + [NII]\lambda\lambda 6548,6583$ intensity ratio between the eastern and western disk emission in UGC3995B is $\gtrsim 2$. An asymmetry of this amplitude is rarely found in published $H\alpha$ images of isolated galaxies, although the distribution and intensity of $H\alpha$ emission is never perfectly symmetric in late type spirals. The enhancement is consistent with the idea that the two galaxies are approaching, primarily, on plane of sky – with the near side gas showing the first evidence of an interaction enhancement.

2) Region UGC 3995-13 in the $H\alpha + [NII]\lambda\lambda 6548,6583$ map is located between the nucleus of B and the bright $H\alpha$ knots discussed in point 1. It cannot be unambiguously assigned to the spiral arms of either galaxy. The radial velocity demonstrates that knot 13 belongs to UGC 3995A and is seen through the disk of B. The ratio $[NII]\lambda 6583/H\alpha \approx 0.4$ suggests that it is an HII region located at the end of a “semi-detached” high surface brightness region (see Fig. 6). It may be therefore part of the “bridge.” Knot 13 is in any case difficult to explain if UGC3995A and B is a chance projection.

3) The northern arm of UGC 3995A has a more diffuse appearance, suggesting the possibility of a perturbation. This is appreciable especially in the POSS plates and in the B image after subtraction of the two dimensional galaxy models (not shown).

4) The bright filament motivated the “bridge” classification in the CPG. As a matter of fact, the bridge appears to be due to: (a) the NW side of the UGC 3995A bar; (b) the “semi detached” high surface brightness region, which includes the NW end of the hammer shaped bar isolated by the eastern arm of UGC 3995A; (c) a region that includes UGC 3995-13, which appears to join the other features to the nucleus of UGC 3995B. A model based on reflection of the unobscured end of the UGC 3995A bar, coupled with the overlapping spiral arms of UGC 3995B, does not entirely explain the extension of the “semi-detached” feature, which may have been tidally deformed. However, the nature of region (c) is not free of ambiguity because the surface brightness measured on the HST image appears to be only marginally higher ($\lesssim 20\%$) than its symmetric counterpart on the western side of UGC 3995B. On the R image, which is contaminated by $H\alpha$ emission, the surface brightness difference is more evident.

5) As noted in § 3.1, the western arm of UGC 3995B appears to extend much farther than its symmetric counterpart. The two arms are reflections of one another for the first 180° of winding. The western arm extends towards component A and crosses the circumnuclear region of that galaxy. It is visible as a prominent dust lane, especially, on the HST image. It is tempting to ascribe the extension as evidence of interaction and

the analogy to the extension of an arm of M51 towards its companion is obvious (e. g., Laurikainen, Salo, & Aparicio 1998). On the other hand, the apparent lack of symmetry for the eastern and western spiral arm of UGC 3995A may be due only to the lack of background emission on the western side of UGC 3995B: the eastern extension of the western arm can be noted only because it adsorbs light from UGC 3995A.

Concluding, the most robust evidence of interaction is due to the brighter $H\alpha$ emission on the eastern side of UGC 3995B, and to region UGC 3995-13, which is right at the end of the high-surface brightness distortion of the bar (see Fig. 6). Other features (points (4) and (5) above) are more ambiguous in their interpretation.

4.3. The Encounter

The relative orientation of UGC 3995A and B is well constrained. The Sc galaxy UGC 3995B is oriented almost face-on ($i \approx 8^\circ$) and is located in front of the SBbc galaxy UGC 3995A ($i \approx 60^\circ$). Component B partially obscures the western side of component A. If spiral arms trail then the northern side of UGC 3995A is the near side. A similar consideration suggests that the southern side of UGC 3995B is nearer. However, the line of nodes for UGC 3995B is unconstrained.

A dominant velocity component along the $E \rightarrow W$ direction would imply a prograde encounter. The system does not show any of the morphological features expected from such a prograde encounter *after* closest approach. The global symmetry of both galaxies is more consistent with an encounter stage before perigalacticon. In this case, the western arm of UGC 3995B could have been really distorted towards UGC 3995A as the two galaxies should have already passed in front of each other on the plane of the sky (see point (5) of §4.2). The observed HI 21 cm profile argues against the prograde encounter scenario, as any velocity perturbation of disk gas (not to be confused with the orbital velocity of the two galaxies) would have to be entirely on the plane of the sky.

The alternative possibility involves a velocity component along the direction $W \rightarrow E$. In this case, the encounter would be retrograde, with the two galaxies either before or after their closest approach. Among interacting Seyfert galaxies, a significant fraction appears to undergo a retrograde encounter (Keel 1996). A retrograde encounter may be as efficient as a prograde one in driving gas from the inner central parsecs of a gas rich galaxy like UGC 3995A toward the central black hole. A retrograde encounter is consistent with the unperturbed appearance of the HI disk, and with the presence of localized star formation in knots along the spiral arms. A retrograde encounter, always assuming that the galaxies are

at, or close to perigalacticon, would not produce large-scale distortions. Test particles in a restricted three body simulation are subject to forces pulling them alternatively inward and outward, with little net result (Binney & Tremaine 1987, Toomre & Toomre 1972). These kind of forces are expected to enhance the probability of molecular cloud collisions, and hence to favor localized star formation especially in spiral arms, as observed in UGC 3995.

The bar appears strong, regular, and dominated by stellar emission. A tidal perturbation due to the proximity of a companion may be enough to induce the formation of such a bar, which is thought to facilitate inflow of gas toward the center (Hunt & Malkan 1999 and references therein). Strong bars are thought to be only a transient phase in the life of galaxy, and form relatively quickly, in a time that can be comparable to the dynamical timescale at the end of the bar of UGC 3995A (Combes & Elmegreen 1993). These results are consistent with our suggestion that the encounter is recent.

In addition, recent work has shown that bars are more frequent in Seyfert 2 than in Seyfert 1 galaxies (Maiolino et al. 1997). Hunt & Malkan 1999 found clear evidence of a sequence of bar incidence that decreases from HII/Starburst galaxies, through LINERs, Seyfert 2 and Seyfert 1. An important conclusion of these authors is that this sequence can be interpreted as an evolutionary sequence in time, dependent also on the interaction strength (or on the strength of any other non-axisymmetric perturbation). UGC 3995 could be seen as an “early” Seyfert 2 according to this scheme.

5. Conclusion

It is most likely that the gaseous component in the eastern part of the disk of UGC 3995B (enhanced H α emission on the side closest to UGC 3995A), and also in the western part of UGC 3995A (NW end of bar, region 13) has been affected by the encounter (see §3 and §4). The relative orientation, motion and morphologies of UGC 3995A and B are most consistent if the two galaxies are not widely separated but are in the early stages of their encounter. The presence of an active nucleus in an early stage encounter apparently does not pose a problem, since gas in the circumnuclear regions may reach the nucleus on time scales comparable to the dynamical timescale (Whittle 1994, and references therein). If the encounter is prograde, then the two galaxies should be before their first closest approach. Otherwise, the galaxy orientation and motions, and especially the unperturbed HI profile are consistent with a retrograde encounter.

We thank W. C. Keel and D. L. Domingue for permission to measure their UGC 3995 spectrum.

REFERENCES

- Begelman, M. C., 1994 in *Mass-Transfer Induced Activity in Galaxies*, (Cambridge: CUP), I. Shosman Ed., 23
- Binney, J. & Tremaine, S., 1987, *Galactic Dynamics* (Princeton: Princeton University Press)
- Blandford, R. D. 1990, in *Active Galactic Nuclei*, (Berlin: Springer) Saas-Fee Advanced Course 20, 161
- Bressan, A., Chiosi, C., & Tantalo R. 1996, *A&A*, 311, 425
- Byun, Y. I. & Freeman, K. C. 1995, *ApJ* 448, 563
- Caon N., Capaccioli M., & D’Onofrio M. 1993, *MNRAS*, 265, 1013
- Chatzichristou, E. T., Vanderriest C. & Lehnert, M. 1998. *A&A* 330, 841
- Combes, F., & Elmegreen, D. M. 1983 *A&A*, 271, 391
- Combes, F. 1997, *IAU Symposia*, 186, in press
- De Robertis, M. M., Yee, H. K. C. & Hayhoe, K. 1998, *ApJ*, 496, 93
- de Vaucouleurs, G. 1959, *AL* 64, 397
- de Vaucouleurs, G., de Vaucouleurs, A., Corwin, H. G., Jr., Buta, R. J., Paturel, G., Fouqué, P. 1991, *Third Reference Catalogue of Bright Galaxies* (New York: Springer)
- Domingue, D., L., Keel, W. C., & White, R. E. III 1998, *ApJ*, in press
- D’Onofrio et al. 1999, in preparation
- Dultzin-Hacyan, D., Marziani, P., & D’ Onofrio, M. 1998, *IAU Symposia*, 186, in press
- Dultzin-Hacyan, D., Fuentes, I., Krongold, Y., & Marziani, P. 1999a, *IAU Symposia*, 186, in press
- Dultzin-Hacyan, D., Fuentes, I., Krongold, Y., & Marziani, P. 1999b, in *Structure and Kinematics of Quasar Broad Line Regions*, Proceeding of a meeting held in Lincoln on March 23-26, 1998, in press.
- Dultzin-Hacyan et al., 1999, in preparation.

Table 1. UGC 3995: Journal of Observations

Date	U. T.	Exp. Time	Filter/Sp. Range (Å)	P. A.
(a) Imaging				
30-Jan-95	06:38	600	R	–
30-Jan-95	06:51	600	R	–
30-Jan-95	07:05	600	R	–
30-Jan-95	07:26	600	H α	–
30-Jan-95	07:50	600	H α	–
30-Jan-95	08:12	600	H α	–
30-Jan-95	08:42	600	B	–
30-Jan-95	08:59	600	B	–
30-Jan-95	09:16	600	B	–
(b) Spectroscopy				
9-dec-1994	9:22	1800	3640–6720	105°
9-dec-1994	9:54	1800	3640–6720	105°
9-dec-1994	10:36	1800	3640–6720	45°
9-dec-1994	11:11	1200	3640–6720	45°
2-feb-1995	07:49	1800	6170–7240	106°
2-feb-1995	08:21	1800	6170–7240	106°
2-feb-1995	08:53	1800	6170–7240	106°
2-feb-1995	09:24	1800	6170–7240	106°
2-feb-1995	10:07	1800	6170–7240	125°
2-feb-1995	10:38	1800	6170–7240	125°
3-feb-1995	07:45	1800	6170–7240	110°
3-feb-1995	08:16	1800	6170–7240	110°
3-feb-1995	08:53	1800	6170–7240	45°
3-feb-1995	09:25	1800	6170–7240	45°
4-feb-1995	07:22	1800	6170–7240	106°
4-feb-1995	07:54	1800	6170–7240	106°
4-feb-1995	08:38	1800	6170–7240	45°

Note. — —: not available or not applicable.

Table 2. Photometric Measurements and Models

Parameter	UGC 3995B	UGC 3995A
Measurements		
B_T		12.5
R_T		11.4
$\langle B - R \rangle$		1.2
Model I		
μ_0	21.00 ± 0.05	19.80 ± 0.05
r_h	12.79 ± 0.64	19.30 ± 0.96
μ_e	22.50 ± 0.05	19.20 ± 0.05
r_e	1.88 ± 0.09	2.66 ± 0.13
$(b/a)_{\text{bulge}}$	1.00 ± 0.05	0.89 ± 0.05
$(b/a)_{\text{disk}}$	1.00 ± 0.05	0.51 ± 0.05
P.A.	0.0 ± 0.10	102.7 ± 0.10
n	1.0 ± 0.05	0.80 ± 0.05
B_{disk}	13.47 ± 0.13	12.10 ± 0.16
B_{bulge}	18.45 ± 0.13	14.60 ± 0.14
B/D	0.01 ± 0.18	0.10 ± 0.21
B_{tot}	13.46 ± 0.18	12.00 ± 0.21
B_{A+B}	11.75 ± 0.21	
Model II		
μ_0	21.62 ± 0.05	20.82 ± 0.05
r_h	12.78 ± 0.64	18.98 ± 0.95
μ_e	23.10 ± 0.05	19.86 ± 0.05
r_e	1.95 ± 0.09	2.99 ± 0.15
$(b/a)_{\text{bulge}}$	1.00 ± 0.05	0.89 ± 0.05
$(b/a)_{\text{disk}}$	1.00 ± 0.05	0.51 ± 0.05
P. A.	0.0 ± 0.10	102.7 ± 0.10
n	1.0 ± 0.05	0.80 ± 0.05
B_{disk}	14.09 ± 0.13	13.16 ± 0.13
B_{bulge}	18.95 ± 0.13	15.01 ± 0.14
B/D	0.01 ± 0.18	0.18 ± 0.21
B_{tot}	14.08 ± 0.18	12.98 ± 0.21
B_{A+B}	12.64 ± 0.21	

Table 3. Narrow Band Photometry: $H\alpha + [NII]\lambda\lambda 6548, 6583$ Fluxes^a

Id.	Angular Distance ^b		Flux	Description
	$\Delta\alpha$	$\Delta\delta$		
1	35	22	5.6	Bright HII on tip of NE spiral arm
2	34	-4	4.9	Two faint HII regions
3	14.3	Bright double HII region
3a	33	-12	...	
3b	30	-15	...	
4	27	4	1.5	Faint HII region
5	14.3	Inner Southern spiral arm
5a	20	0	...	
5b	19	-6	...	
5c	10	-11	...	
5d	3	-13	...	
6	14.9	Diffuse emission from SE spiral arm
6a	17	-21	...	
6b	12	-22	...	
7	0	0	112	Nucleus UGC 3995A
8	-5	22	3.4	HII region on northern arm
9	12.8	Two HII region, one faint
9a	-9	14	...	
9b	-10	16	...	
10	-13	4	2.9	HII region nearly aligned with the nuclei of UGC 3995A and B
11	-16	0	2.7	Bright HII region on the pseudo-ring
12	-20	18	7.9	Bright HII region on northern arm
13	-20	9	10.4	Bright knot at center of pseudo-ring
14	-23	3	3.2	HII region on south arc of the pseudo-ring
15	-28	6	7.1	Nucleus of UGC 3995B
16	-28	-3	6.9	Bright HII region on south arc of the pseudo-ring
17	-31	12	3.7	HII region
18	-35	5	4.5	Faint HII regions close to UGC 3995B
19	-44	8	2.1	Faint HII region on western arm of UGC 3995B
–	–	–	572	Total $H\alpha + [NII]\lambda\lambda 6548, 6583$ flux

^aIn units of 10^{-15} ergs s^{-1} . Fluxes are uncorrected for internal absorption, and for galactic extinction: for $A_B \approx 0.09$, the resulting $H\alpha + [NII]\lambda\lambda 6548, 6583$ fluxes should be higher by 5 %, an increment that is smaller than the uncertainties associated to the calibration.

^bIn seconds of arcs, measured from the $H\alpha$ centroid of the Seyfert nucleus (region 7); $\Delta\alpha$ and $\Delta\delta$ are positive to the east and to the north respectively.

Table 4. Emission Lines Fluxes and Widths

Line Id.	UGC 3995A		UGC 3995B	
	Flux	FWHM ^a	Flux	FWHM ^a
HeII λ 4686	2.7:
H β	6.3	350 ^b
[OIII] λ 4959	19.1	380
[OIII] λ 5007	55.8	340 ^b
[NII] λ 6548
H α	23.22	370	1.4	$\lesssim 100$
[NII] λ 6583	22.93	370	0.6	$\lesssim 100$
[SII] λ 6716	6.8	320	0.25:	$\lesssim 100$
[SII] λ 6730	6.4	330	0.22:	...

^aFWHM values have been corrected for instrumental width, assuming $\text{FWHM}_{\text{instr}} \approx 410 \text{ km s}^{-1}$, for the H β and [OIII] λ 4959,5007 lines, and $\approx 100 \text{ km s}^{-1}$ for the H α and [NII] λ 6548,6583 lines from the measurement of faint comparison and sky lines.

Note. — ... : not revealed or not measured due to poor quality. “:”: highly uncertain.

- Hodge, P. W. 1975a, ApJ 201, 556
- Hodge, P. W. 1975b, ApJ 202, 619
- Hodge, P. W. & Kennicutt, R. C., J. 1983, AJ, 88, 296
- Holmberg, E. 1958, Medd. Lund Ser. II, No. 136
- Hunt, L. K., & Malkan, M. A. M. 1999, ApJ, in press (SISSA preprint number astro-ph/9901410)
- James, P. A., & Puxley, P. J. 1993, Nature 363, 240
- Karachentseva, V. E. 1973, The catalogue of isolated galaxies., Soobshcheniya Spetsial'noj Astrofizicheskoy Observatorii, 8, 3
- Karachentseva V.E., Karachentsev I.D., Lebedev V.S. 1988, Astrof. Issledovanija Byu. Spec. Ast. Obs., 26, 42
- Keel, W. C. 1985, AJ 90, 2207
- Keel, W. C. 1996, AJ 111, 696
- Kennicutt, R. C., J., Edgar, B. K., & Hodge, P. W. 1989, ApJ, 337, 761
- Kennicutt, R. C. 1992, ApJS 79, 255
- Laurikainen, E., & Salo, H. 1995, A&A, 293, 683
- Laurikainen, E., Salo, H. & Aparicio, A. 1998, A&AS 129, 517
- Maiolino, R., Ruiz, M., Rieke, G. H., & Papadopoulos, P. 1997, ApJ, 485, 552
- Malkan, M. A., Gorjian, V., & Tam, R. 1998, ApJS, 117, 25
- Marquez, I., & Moles, M. 1994, AJ 108, 90
- Marziani, P. 1995, IA-UNAM Internal Report CI-95-04
- Odehahn, S. C., Bryja, C., Humphreys, R. M. 1992, PASP 104, 553
- Osterbrock, D. E. 1993, ApJ, 404, 551
- Pronik, I. I. & Metik, L. 1990, , NASA, Marshall Space Flight Center, Paired and Interacting Galaxies: IAU Colloquium No. 124, 331

- Rafanelli, P., & Marziani, P., 1992, AJ 103, 743
- Rubin, V. C., Ford, W. K., & Thonnard, N. 1980, ApJ 238, 471
- Ryder, S. D. & Dopita, M. A. 1993, ApJS, 88, 415
- Schweizer, F., & Thonnard, N. 1985, PASP, 97, 104
- Stockton, A. 1999, IAU Symposia, 186, in press.
- Sulentic, J. W. & Arp, H. 1983, AJ, 89, 489
- Toomre, A., & Toomre, J. 1972, ApJ 178, 623
- Valentijn, E. A. 1990, Nature 346, 153
- White, R. E., & Keel, W. C. 1992, Nature, 359, 129
- Whittle, M, 1994 in Mass-Transfer Induced Activity in Galaxies, (Cambridge: CUP), I.
Shosman Ed., 63

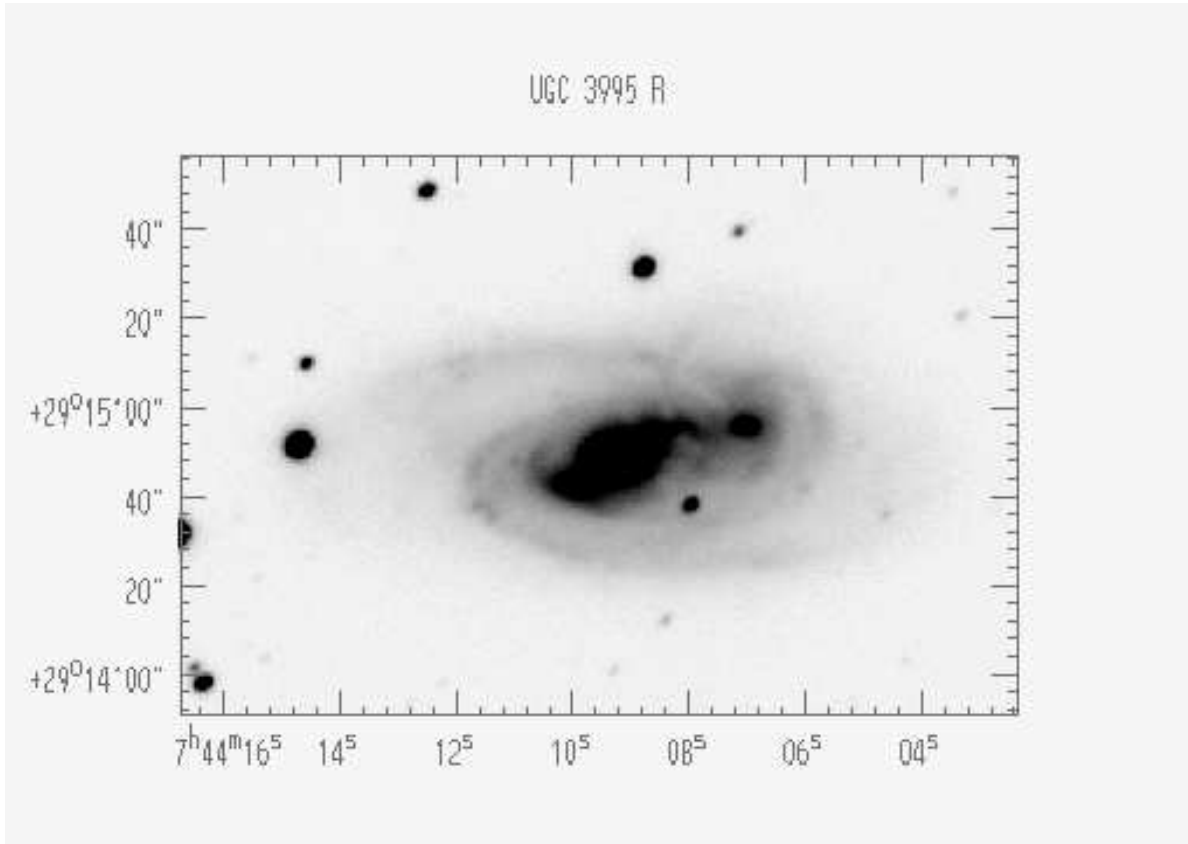


Fig. 1.— Johnson R image of the UGC 3995 system (the average of three 600^s exposures. Note the perturbed appearance of the bar in the contact region between the two components, and the bright filament that seems to connect their nuclei. In this and the following labeled images, Right Ascension (abscissa scale) and Declination are referred to J2000.

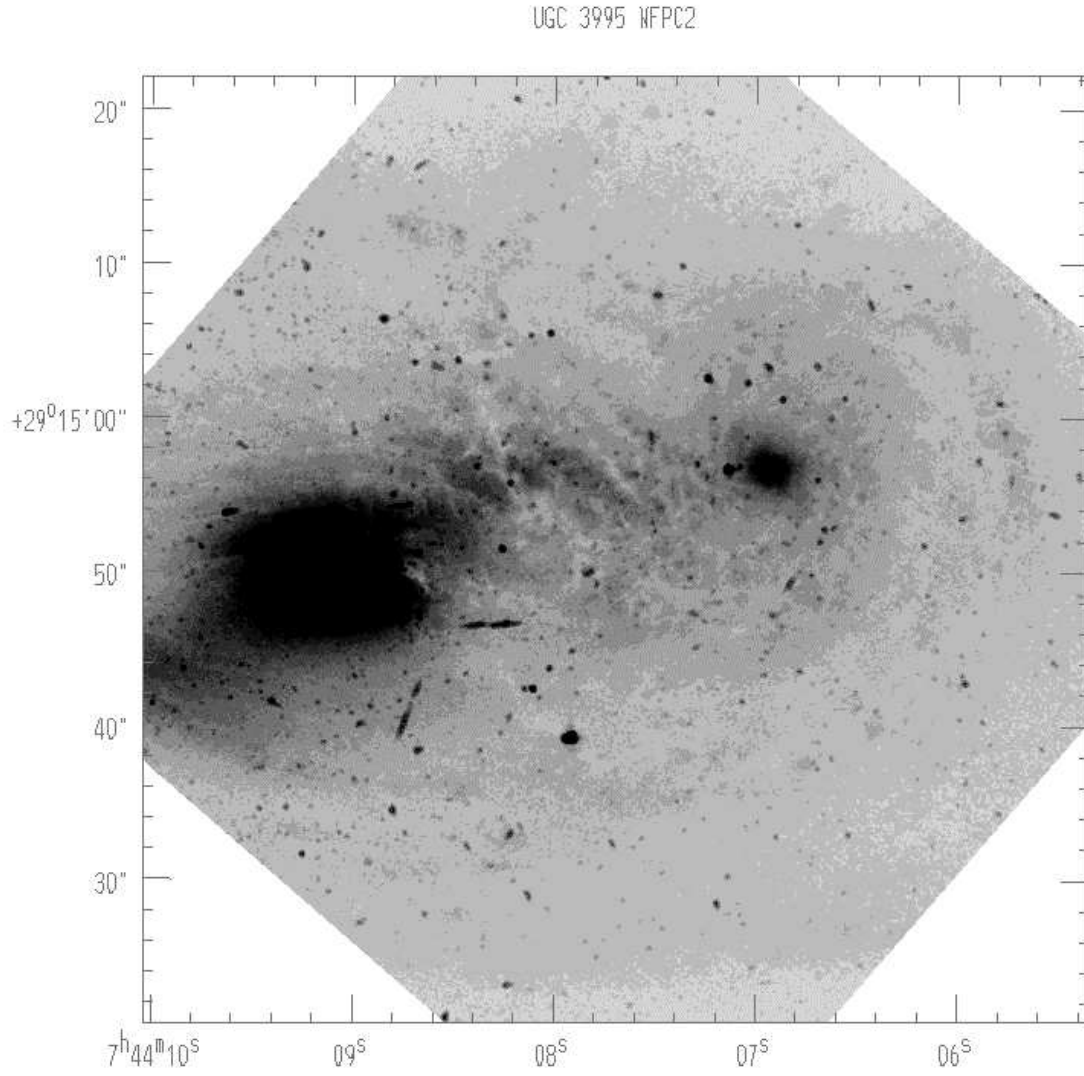


Fig. 2.— WFPC2 image of the UGC 3995 system obtained through the wide visual F606W filter, after mosaicing and rotation by 49°. Cosmic rays have been partially removed following standard procedures.

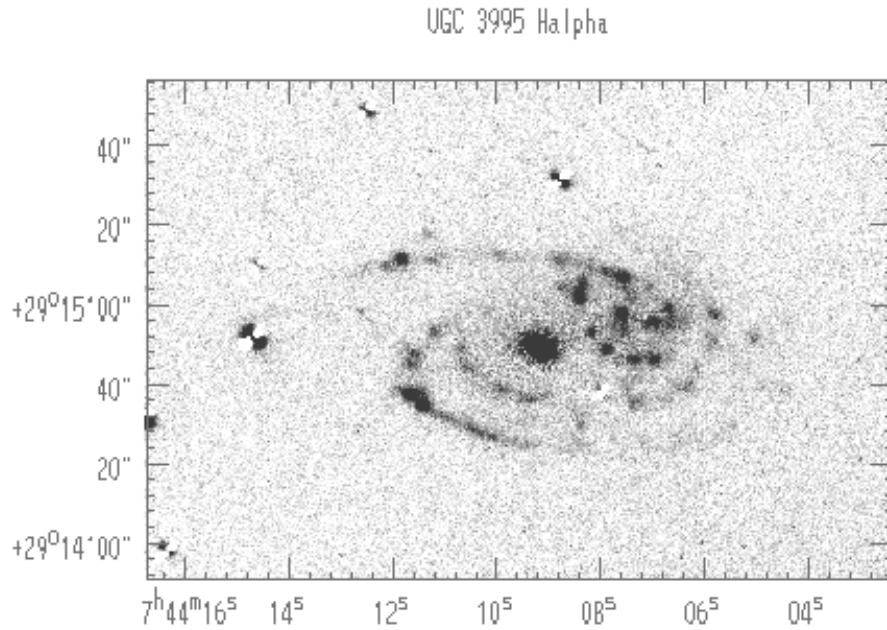


Fig. 3.— $H\alpha + [NII]\lambda\lambda 6548, 6583$ continuum-subtracted image of UGC 3995. The image is the average of three 1200^s exposures. The continuum underlying $H\alpha$ and $[NII]\lambda\lambda 6548, 6583$ has been subtracted as a scaled R image. Strong stars show bow tie residuals, probably because of slight difference in seeing or of small guiding errors at the time the narrow and R band images were collected.

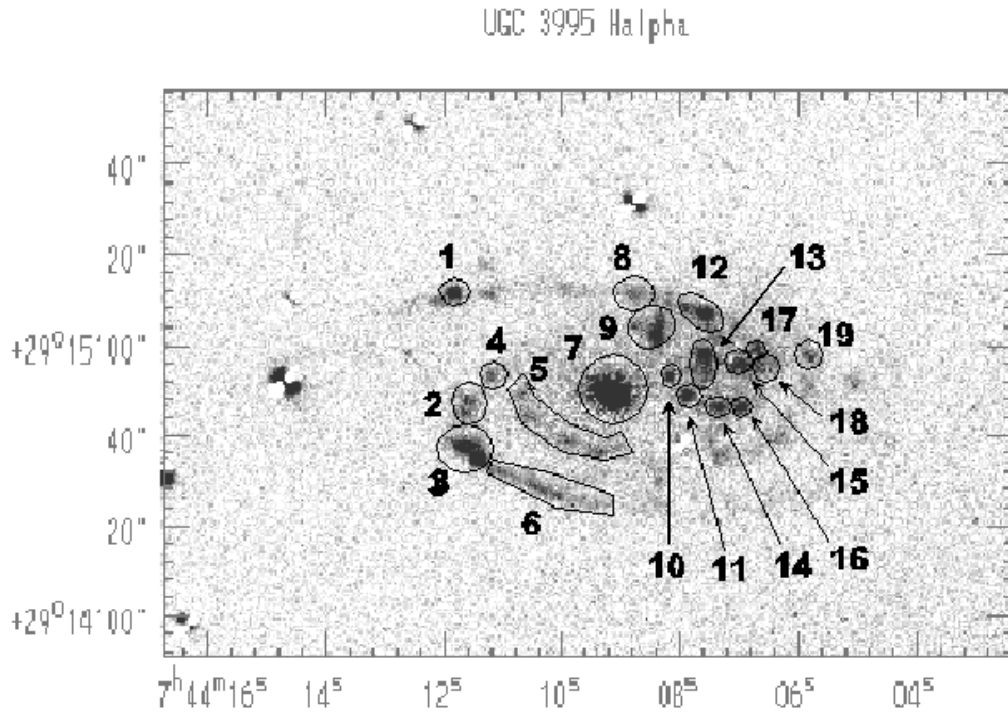


Fig. 4.— H α + [NII] $\lambda\lambda$ 6548,6583 continuum-subtracted image of UGC 3995, same as Fig. 3. Labels have been assigned in order of decreasing rights ascension. Fluxes and a short description of each emitting region are reported in Table 3

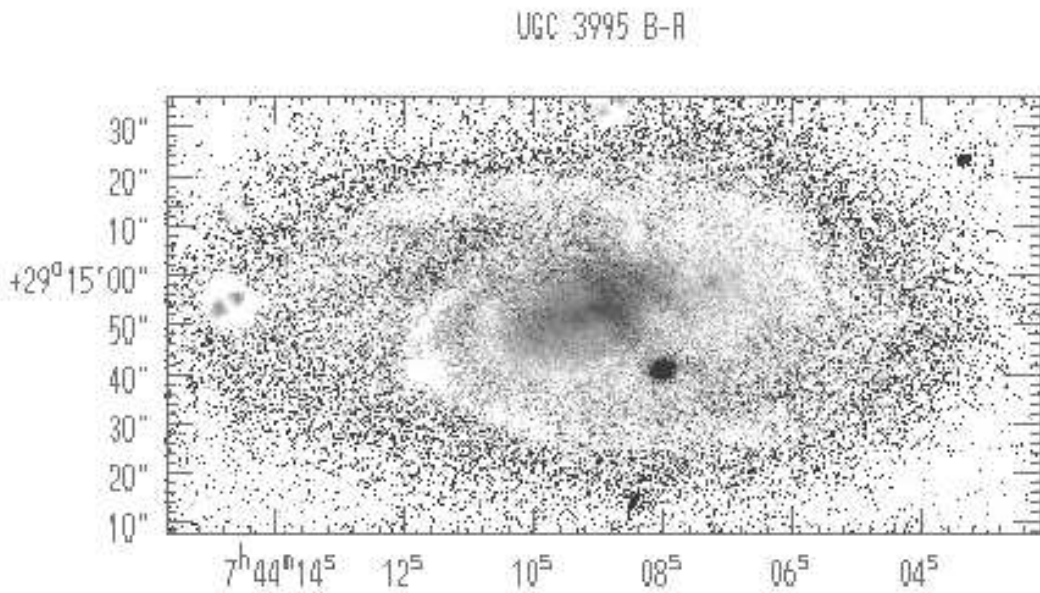


Fig. 5.— UGC 3995 color map ($B - R$). The color range displayed is approximately 0.0 (white) $\lesssim B - R \lesssim 1.5$ (black). $B - R$ values in correspondence of UGC 3995B are $\approx 0.7 - 0.8$, suggesting that UGC 3995B is located in front of UGC 3995A. The red spot ($B - R \approx 2.0$) south of the Seyfert nucleus is likely a foreground star.

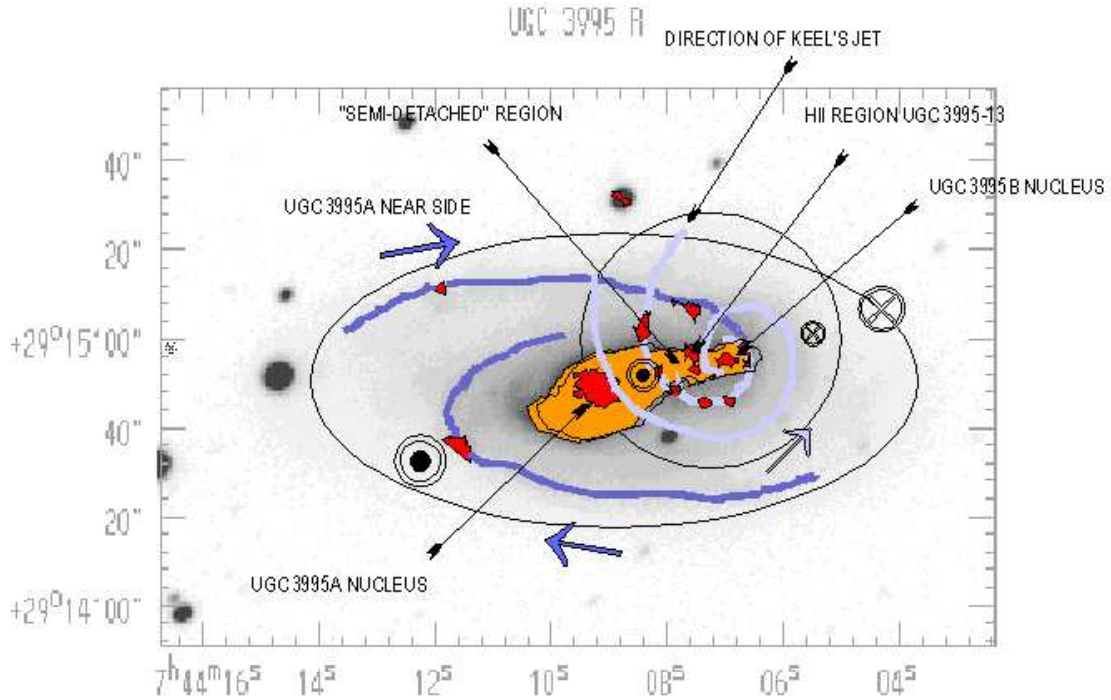


Fig. 6.— Graphical sketch of the UGC 3995 system. Orange color: bar and filament connecting the nuclei of UGC 3995A and B, the highest surface brightness region of the system. Dark blue: spiral arms of UGC 3995A; light blue: spiral arms of UGC 3995B. Red: emitting regions as in $H\alpha + [NII]\lambda\lambda 6548, 6583$ map; The \odot marks negative radial velocity; the \otimes symbol positive radial velocity. The large symbols are for UGC 3995A. The “jet” (Keel 1985) appears to be associated with a spiral arm of UGC 3995B that extends toward objects which are, most likely, a foreground star, and a very faint background galaxy (Chatzichristou, Vanderriest & Lehnert 1998).

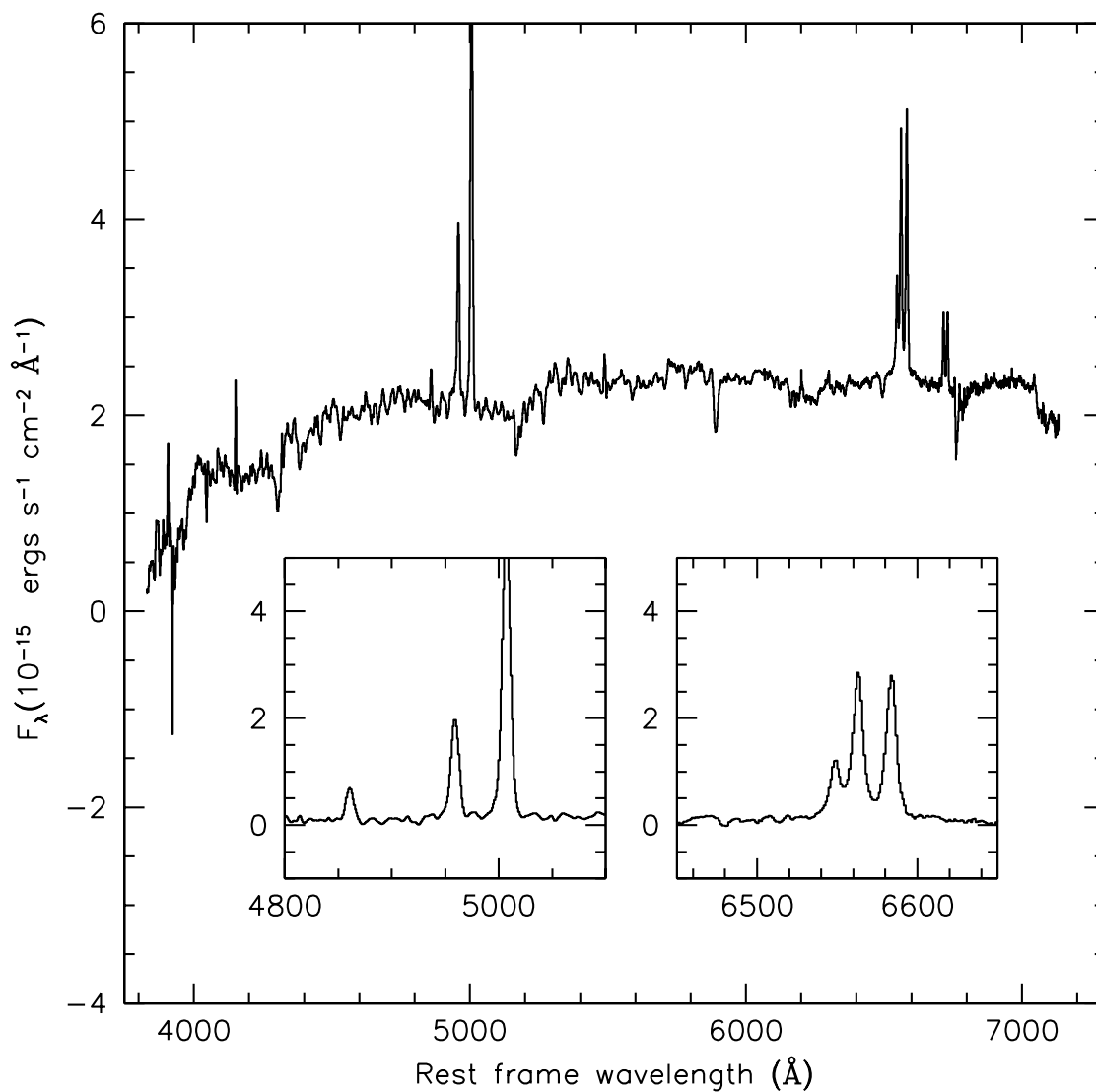


Fig. 7.— De-redshifted nuclear spectrum of UGC 3995. Abscissa scale is wavelength, ordinate scale is specific flux multiplied by 10^{15} . The two smaller inlets show the H β and [OIII] λ 4959,5007 region (left) and the H α + [NII] λ 6548,6583 blend (right) after subtraction of the galaxy absorption spectrum, modeled employing a scaled spectrum of NGC 3379, obtained from Kennicutt’s digital spectrophotometric atlas of galaxies (Kennicutt 1992).

UGC 3995 P.A.=106

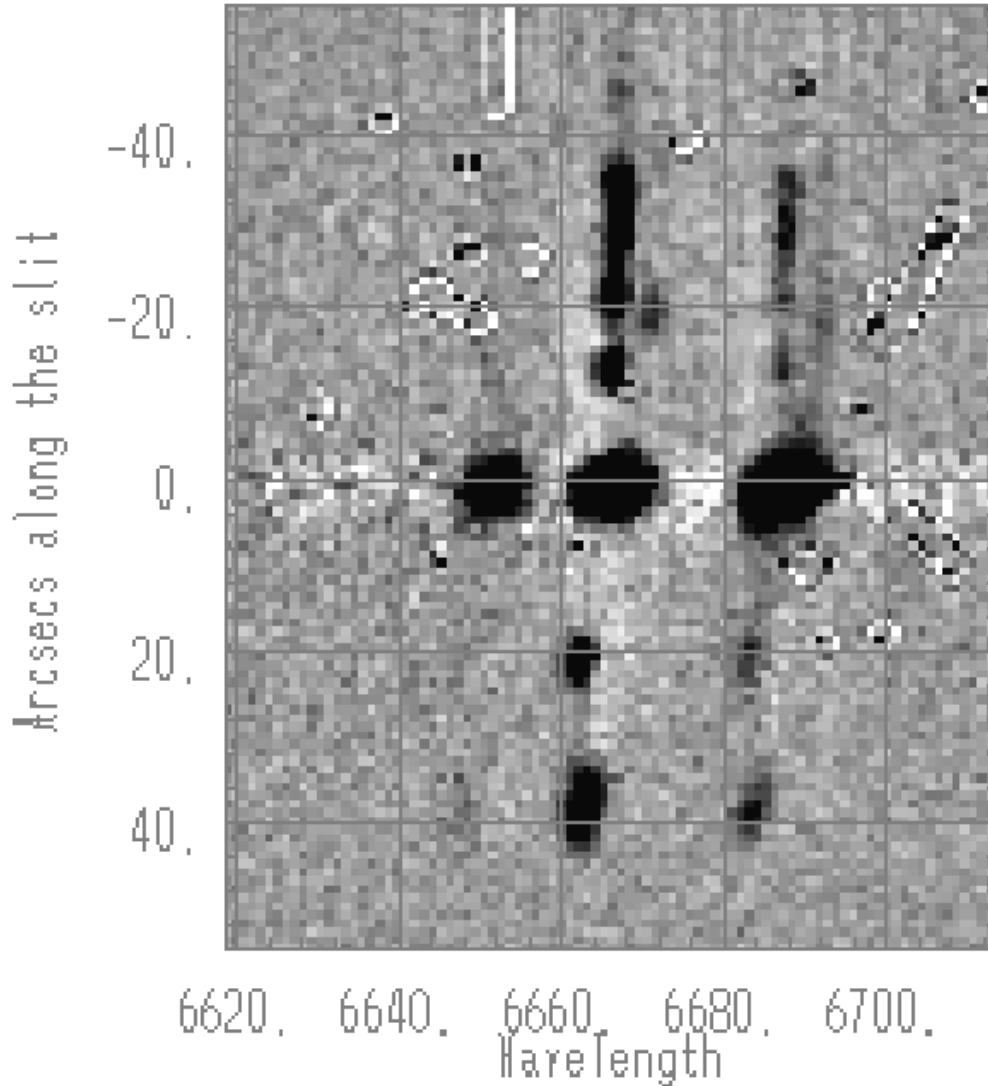


Fig. 8.— Long slit spectrum at P. A. = 106° , with both galaxy nuclei in the slit. Abscissa is wavelength in \AA ; ordinate is arcsecs along the slit. The zero-point of the angular scale has been set at the position of the Seyfert nucleus. The spectrum is the average of four 1800^s exposures obtained sequentially, cleaned for cosmic rays. The scale of intensity has been set to show the important details at a level which is just $\approx 6\sigma$ the noise level. The galaxy stellar and the AGN continuum have been removed employing a median filter to better show the structure of the extended emitting regions.

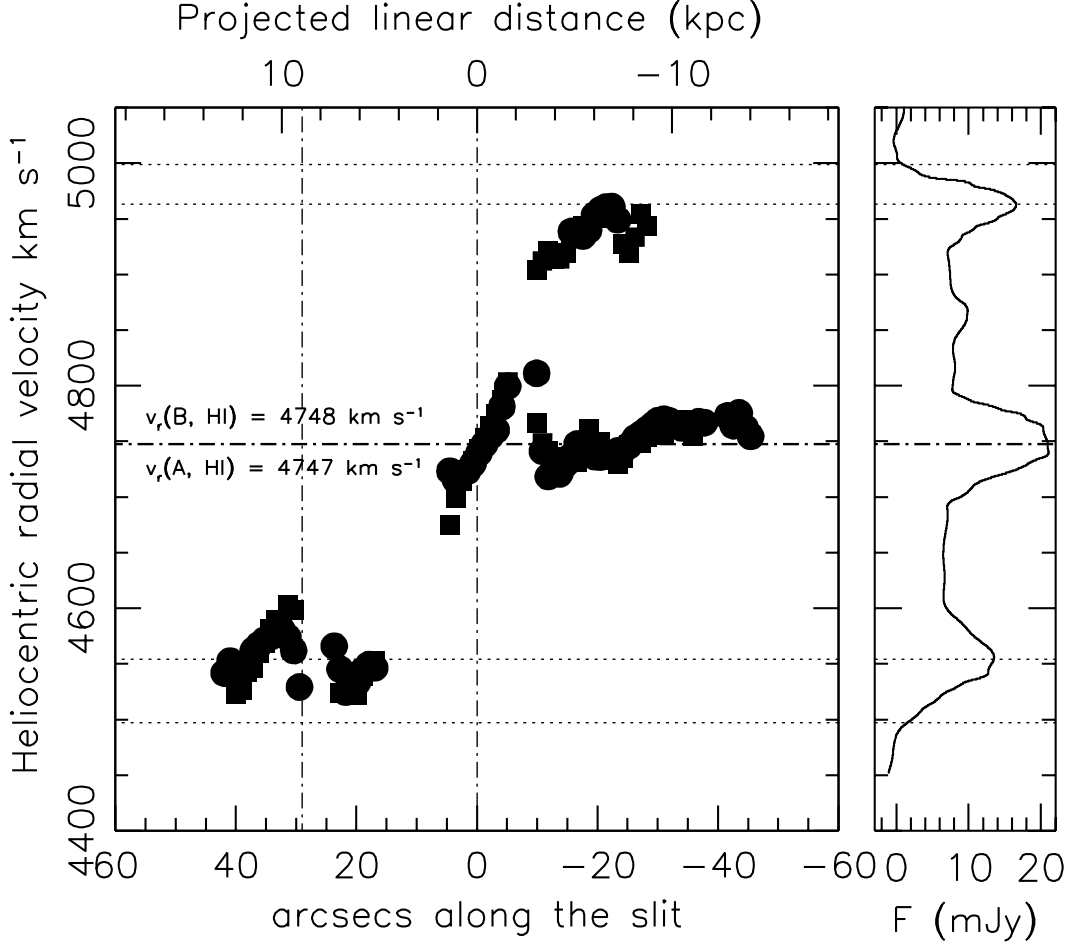


Fig. 9.— Left Panel – Radial velocity curve at P. A. = 106°. The abscissa scale is arcsecs (lower axis) and projected linear distance (upper axis) along the slit increasing to the West (the zero point of the angular and spatial scale has been set at the position of the Seyfert nucleus), the ordinate scale is heliocentric radial velocity in km s⁻¹. Filled circles: H α measurements; filled squares: [NII] λ 6583 measurements. Uncertainties associated with measurements are estimated to be, at a 2 σ confidence level, ± 50 km s⁻¹ for the obscured UGC 3995A emission at $v_r \approx 4950$ km s⁻¹, ± 10 km s⁻¹ for measurements in the nuclear region and of the UGC 3995B H α line, and approximately ± 30 km s⁻¹ in all other cases. The horizontal dotted-dashed lines are the heliocentric radial velocities for UGC 3995A and 3995B, from the 21 cm HI profile of Sulentic & Arp 1983. The dotted lines are the heliocentric radial velocities of the “horn” peaks and of the 20 % intensity level in the 21 cm line profile. In correspondence of UGC 3995B, gas from both UGC 3995A and UGC 3995B is detected. The lower radial velocity part of the velocity curve is from gas associated with UGC 3995B. Right Panel – HI 21 cm line profile; ordinate is radial velocity as for the right panel; abscissa

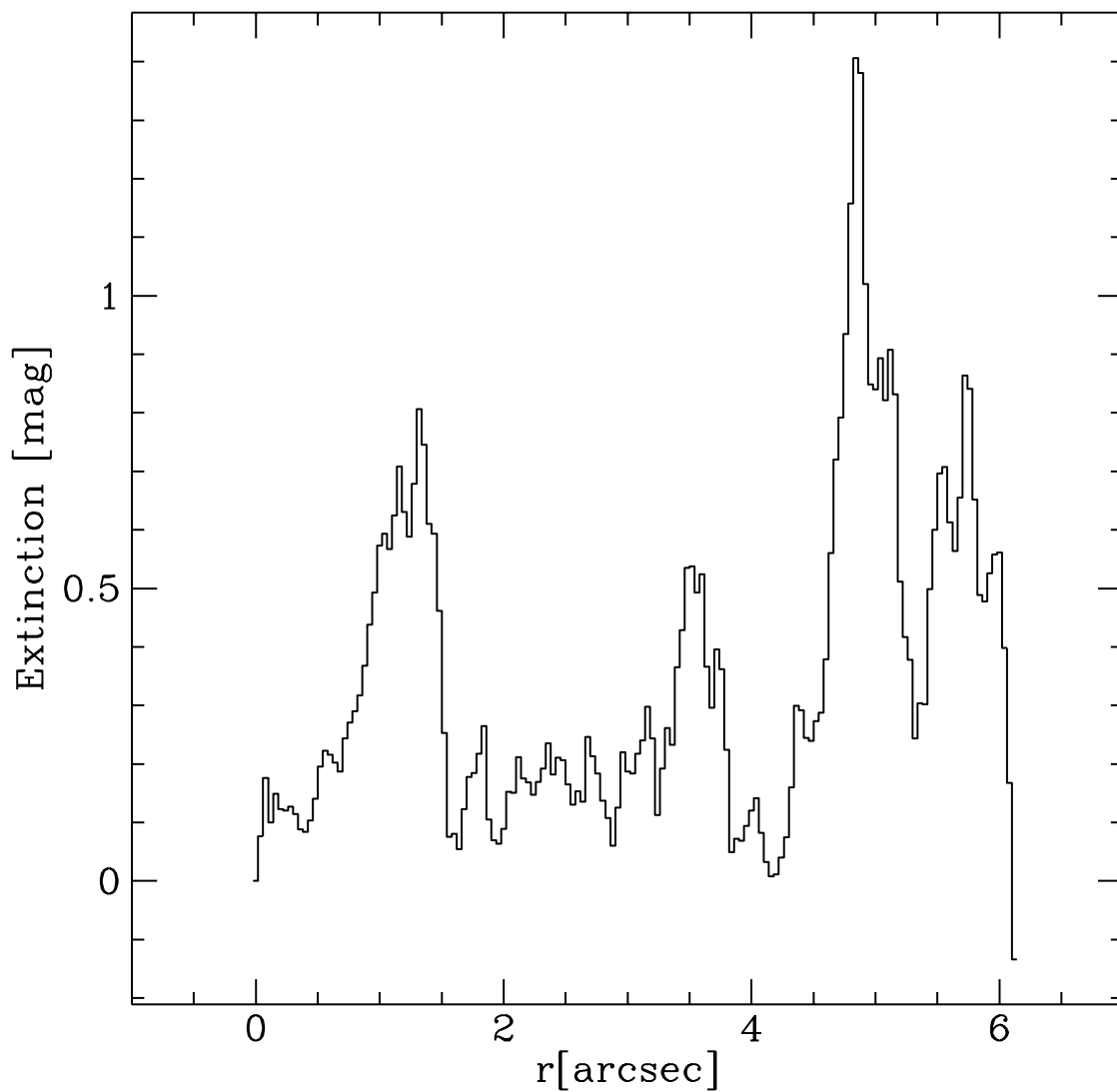


Fig. 10.— Extinction profile along the bar of UGC 3995, measured on the WFPC2 image, in wide-V magnitudes ($2.5\log(I_{\text{unobscured}}/I_{\text{obscured}})$). The origin of the abscissa scale has been set at the Seyfert nucleus of UGC 3995A. Angular distance d'' is increasing toward the NW; at $d'' \approx 1$ the absorption peak is associated with the eastern extension of the western spiral; at $d'' \approx 5$ the peak of absorption is due to the eastern spiral arm.